

ARTICLE

Received 28 Jun 2013 | Accepted 10 Feb 2014 | Published 4 Mar 2014

DOI: 10.1038/ncomms4422

Transition-metal-substituted polyoxometalate derivatives as functional anti-amyloid agents for Alzheimer's disease

Nan Gao¹, Hanjun Sun¹, Kai Dong¹, Jinsong Ren¹, Taicheng Duan¹, Can Xu¹ & Xiaogang Qu¹

Inhibitions of amyloid β ($A\beta$) aggregation and $A\beta$ -haem peroxidase-like activity have received much attention because these two symptoms can be the primary targets of therapeutic strategies for Alzheimer's disease (AD). Recently, our group found that polyoxometalate (POM) with a Wells–Dawson structure can efficiently inhibit $A\beta$ aggregation. However, the interaction between POMs and $A\beta$ is robust, but still needs to improve $A\beta$ binding affinity. More importantly, it is unclear whether POMs can cross the blood–brain barrier and decrease $A\beta$ -haem peroxidase-like activity. Here we show that our designed series of transition metal-functionalized POM derivatives with a defined histidine-chelated binding site have much better $A\beta$ inhibition and peroxidase-like activity inhibition effects than the parent POM. More intriguingly, we show that these compounds can cross the blood–brain barrier and are metabolized after 48 h. Our work provides insights into the design, synthesis and screening of inorganic metal compounds as multifunctional therapeutic agents against AD.

¹Division of Biological Inorganic Chemistry, State Key Laboratory of Rare Earth Resource Utilization and Laboratory of Chemical Biology, Changchun Institute of Applied Chemistry, University of Chinese Academy of Sciences, Chinese Academy of Sciences, Changchun, Jilin 130022, China. Correspondence and requests for materials should be addressed to X.Q. (email: xqu@ciac.ac.cn).

Alzheimer's disease (AD) is characterized by cerebral extracellular amyloid plaques and intracellular neurofibrillary tangles¹. Although the molecular mechanisms of AD pathogenesis are not clearly understood owing to its complexity, recent studies have demonstrated that the polymerization of amyloid β -peptides ($A\beta$) into amyloid fibrils is crucial^{1–3}. Therefore, the design, synthesis and screening of $A\beta$ aggregation inhibitors have received much attention for the therapeutic and preventive treatment of AD.

Since the discovery of the antitumor activity of cisplatin, a number of inorganic metal compounds have been used as important therapeutic agents and diagnostic imaging probes^{4–15}. Worldwide sales of inorganic drugs are rapidly increasing. However, few inorganic agents have been reported that can inhibit $A\beta$ amyloid formation^{6–11}. Polyoxometalates (POMs) are early transition metal oxide clusters (especially Mo, W and V) with high oxidation states, and they are used for constructing molecular architectures with potential applications¹⁶, for example, in catalysis¹⁷, magnetic materials¹⁸, chiral recognition¹⁹ or nanocomposites²⁰. Furthermore, POMs are promising candidates for drug-carrier approaches on the way to new composite drugs because they have long been known for their multifaceted bioactivity that encompasses antiviral, anticancer, antibacterial and herbicidal properties²¹. Some functionalized POMs have been used as inhibitors of HIV-1 protease²¹ or the DNA-binding activity of Sox2 (ref. 22). Most recently, our group has reported that POMs can be excellent inhibitors to the aggregation of $A\beta$, and, among them, the phosphotungstate with a Wells–Dawson structure (POM-Dawson) has the strongest inhibition effect²³. However, the interactions between POMs and $A\beta$ are mainly dependent on favourable electrostatic attraction and POM size effects, which are robust but not specific. For increasing the specificity of POMs binding to $A\beta$ with improved cytotoxicity, it is important and feasible to modify POM-Dawson by introducing a specific $A\beta$ recognition factor. According to previous results, POMs target the cationic cluster from His13 to Lys16 (HHQK) on $A\beta$ ²³. Notably, this cluster contains two adjacent histidines, which can specifically chelate transition metal ions, such as Ni(II) or Co(II)^{24–27}. Therefore, histidine can be a potential chelating site for POMs to improve their specific recognition of $A\beta$. As a result, POMs with a defined histidine-chelating site may enhance their $A\beta$ inhibition effects.

Moreover, it was not safe enough when $A\beta$ peptides were just inhibited, since recently it has been reported that haem binds to $A\beta$ monomers, which may play another major role in AD. The $A\beta$ -haem complex is shown to be a peroxidase, which catalyses the oxidation of serotonin and 3,4-dihydroxyphenylalanine by reactive oxygen species. In the native human $A\beta$ peptides, either His13 or His14 can coordinate to haem and His13 probably binds haem specifically. Mutating the His13 and His14 residues simultaneously can prohibit haem binding, inducing loss of peroxidase-like activity^{28–30}. Therefore, a strong affinity between an inhibitor and His13 and His14 will suppress the peroxidase-like activity, which could potentially be useful in the treatment of AD. Moreover, few inorganic agents have been reported that can inhibit the $A\beta$ -haem peroxidase-like activity^{28,30}.

However, it is unclear whether transition metal substitution in POM will reveal the best effects. We therefore introduced a semi-rational design approach for our studies. A semi-rational design is a widely used intermediate approach that involves the identification of important residues in a biological enzyme³¹. Here, we describe a series of transition metal-functionalized POM-Dawson derivatives (POMDs) with various well-known histidine-chelating metals (such as Cu, Fe, Ni, Co and Mn) (Fig. 1) by using high-throughput screening to verify the improvement in the binding affinity of the POMDs to $A\beta$. As designed, POMDs would have

much better capability to inhibit $A\beta$ fibril formation and $A\beta$ -mediated peroxidase-like activity. In this way, POMDs may act as inorganic dual-functional anti- $A\beta$ agents for the therapy of AD.

Results

Characterizations of POM and POMDs. All POM-Dawson and POMDs were synthesized and characterized as previously described (Supplementary Figs 1,2 and Supplementary Tables 1,2)³². To identify the capabilities of POM-Dawson and five POMDs in inhibiting $A\beta$ aggregation, a high-throughput screening method was used. The screen used a fusion of $A\beta$ 42 to enhanced cyan fluorescent protein ($A\beta$ -ECFP). In the absence of inhibition, the rapid misfolding and aggregation of $A\beta$ 42 causes the entire fusion protein to misfold, thereby preventing fluorescence. Compounds that inhibit $A\beta$ 42 aggregation enable CFP to fold into its native structure and be identified by the resulting fluorescent signal (Fig. 2)³³. By using this system constructed in our laboratory²³, we identified POM-Dawson and five POMDs capable of inhibiting $A\beta$ aggregation (Fig. 2). All six compounds could increase the fluorescence, indicating that they prevented $A\beta$ aggregation; among the five POMDs, only POMDs with Ni or Co showed better inhibitory effects than those of unmodified POM-Dawson (Fig. 3). This could be explained as the following. As POM-Dawson targets the HHQK cluster of $A\beta$ ²³, and Ni and Co are well known to possess high binding affinity to histidine^{24–27}, Ni- or Co-metalized POMDs would possess better inhibitory effects. On the basis of the screening results, $K_8P_2NiW_{17}O_{61}$ (POMDs-Dawson-Ni) and $K_8P_2CoW_{17}O_{61}$ (POMDs-Dawson-Co) were used in the following studies.

Stability of POM and POMDs. One issue that needs to be addressed is the stability of the POM and POMDs under our experimental conditions²³. Thus, the stability of POM-Dawson, POMDs-Dawson-Ni and POMDs-Dawson-Co was studied by using UV/Vis spectroscopy (Supplementary Fig. 3), mass spectrometry (MS) (Supplementary Fig. 4) and ³¹P NMR spectroscopy (Supplementary Fig. 5). The results indicated that all of the POM and POMDs used remained intact^{23,32}. Furthermore, the stability of POM and POMDs in the presence of $A\beta$ was also determined by using matrix-assisted laser desorption/ionization time-of-flight (MALDI-TOF) MS (Supplementary Fig. 6). The results indicated that all the POM/POMDs and $A\beta$ peptides remained intact.

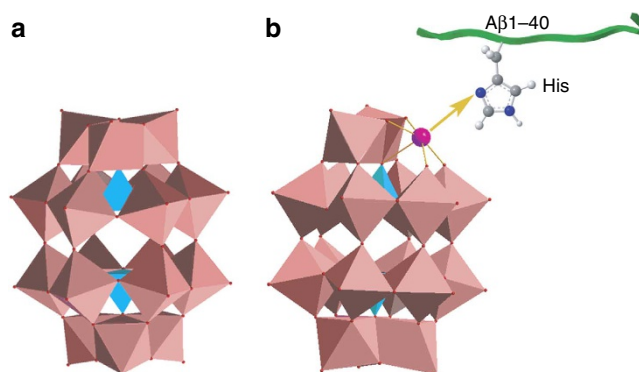


Figure 1 | Structures of POM and POMDs. (a) Wells-Dawson structure; (b) Wells-Dawson POMDs with defined histidine-chelating metals (such as Ni, Co, Cu, Fe and Mn). The PO_4 and WO_6 polyhedra are shown in blue and light pink, respectively. The histidine-chelating metal is shown as a purple ball. The O, C, N and H atoms are shown as red, grey, dark blue and white balls, respectively.

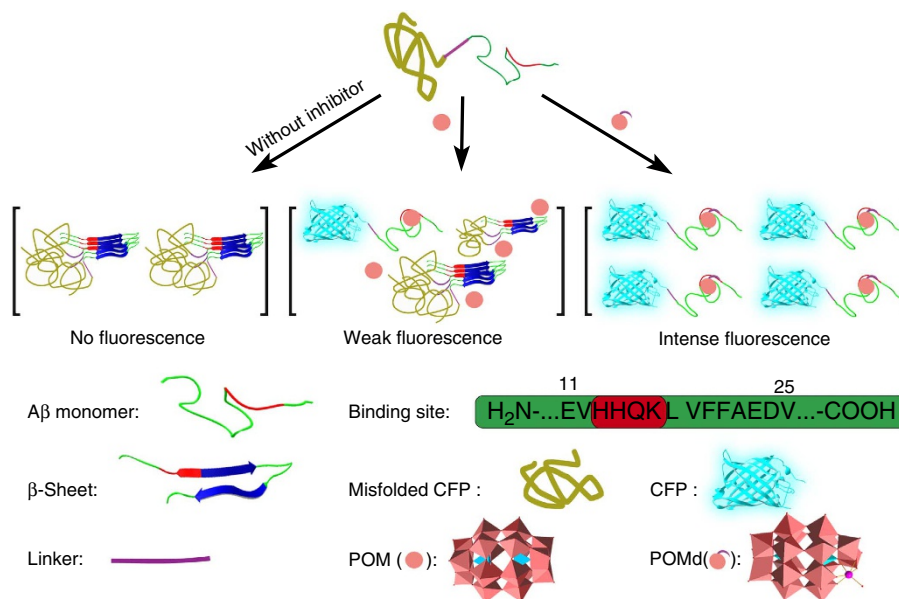


Figure 2 | Schematic illustration of the high-throughput screening method for identifying effective A β -aggregation inhibitors. In the absence of inhibitors, the A β 42 portion of the fusion aggregates rapidly and causes the entire A β 42-ECFP fusion to misfold and aggregate (left). Therefore, no fluorescence is observed. However, inhibition of A β 42 aggregation enables CFP to form its native fluorescent structure (middle, right).

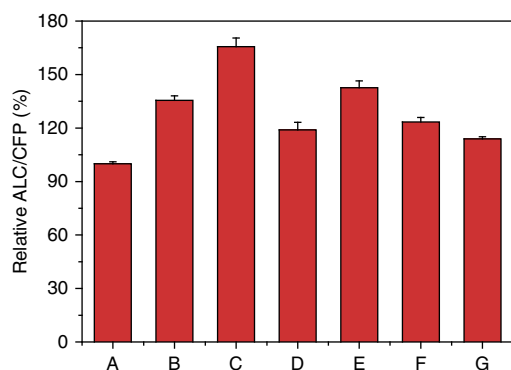


Figure 3 | ECFP-based screening of A β aggregation inhibitors in living *E. coli* cells. A to G: control (without POMs), Dawson-POM, Dawson-POM-Ni, Dawson-POM-Mn, Dawson-POM-Co, Dawson-POM-Cu, Dawson-POM-Fe. % ALC/CFP means percentage of the fluorescence intensity of *E. coli* cells expressing ALC divided by the fluorescence of *E. coli* cells expressing CFP. Data represent the average of three replicate experiments and the error bars indicate the \pm s.d.

Inhibitory effects of POMds on A β aggregation. To verify the inhibitory effects of POMds metallated with Ni or Co on A β aggregation, we used a commonly used *in vitro* thioflavin T (ThT) fluorescence assay to perform further studies²³. ThT, an extrinsic fluorescent dye, is able to bind to amyloid aggregates; upon binding, its fluorescence intensity increases. The formation of amyloid fibrils was quantified by measuring the fluorescence intensity of ThT at 480 nm upon excitation at 444 nm, and POM alone did not affect the ThT fluorescence under our experimental conditions. When fresh A β 1-40 was incubated alone at 37 °C, the ThT fluorescence, as a function of the incubation time, showed a sigmoidal shape. This result was consistent with the nucleation-dependent polymerization model^{34–37}. However, in the presence of POMds-Dawson-Ni or POMds-Dawson-Co the ThT fluorescence was hardly changed, especially for POMds-Dawson-Ni, indicating that the formation of A β amyloid fibrils was suppressed (Fig. 4a). The inhibitory effect followed the

order POMds-Dawson-Ni > POMds-Dawson-Co > POM-Dawson, which was in agreement with the high-throughput screening results. To compare the inhibitory effects, a previously reported pentapeptide-based fibrillogenesis inhibitor, LPPFD³⁸, was used as a positive control (Supplementary Fig. 7). The inhibitory effect of LPPFD was lower than those of all POM and POMd inhibitors. Furthermore, after incubation for 7 days, gel electrophoresis indicated that A β 1–40 in the absence of POMds had aggregated into higher-order oligomers and fibrils (Fig. 4b, lane 2)^{39,40}. In contrast, the formation of A β aggregates was markedly inhibited by POMds-Dawson-Co or POMds-Dawson-Ni, as shown by a stronger monomer band and a weaker aggregate band in the native gel (Fig. 4b, lanes 4, 5), indicating that A β aggregation was inhibited.

We also investigated the effects of POMds-Dawson-Ni and POMds-Dawson-Co on the morphology of A β aggregates using atomic force microscopy (AFM)^{39,40}. Forty micromolar A β was incubated in the absence or presence of POMds-Dawson-Ni or POMds-Dawson-Co in buffer (10 mM HEPES, 150 mM NaCl, pH 7.4) at 37 °C for 7 days. A β formed long unbranched aggregates (Supplementary Fig. 8). In contrast, in the presence of POMds-Dawson-Ni (20 μ M), spherical structures with average heights of 2–3 nm were formed. These results further supported the ThT experiments and indicated that POMds-Dawson-Ni could inhibit the formation of A β fibrils.

To better compare the inhibitory effects of POM-Dawson, POMds-Dawson-Ni and POMds-Dawson-Co, we evaluated their IC₅₀ values using a ThT assay (Supplementary Fig. 9)^{39,40}. Table 1 summarizes their IC₅₀ values. The results indicated that the IC₅₀ values of POMds-Dawson-Ni and POMds-Dawson-Co were approximately 4.5-fold and 1.7-fold lower than that of POM-Dawson, respectively (Table 1). In contrast, the peptide LPPFD (15.60 \pm 1.79 μ M) (error bars indicate \pm s.d., see Supplementary Fig. 9) was similar to that of POMds-Dawson-Co and higher than that of POMds-Dawson-Ni. The results suggested that the inhibition efficiency of POMds-Dawson-Ni and POMds-Dawson-Co was significantly increased due to the strong chelation between Ni or Co and the histidine of HHQK.

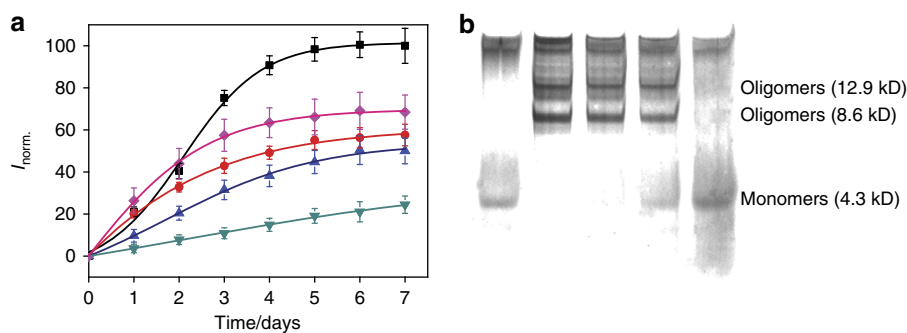


Figure 4 | Inhibition of A β assembly by POMds. (a) Aggregation kinetics of A β 1–40 monitored by ThT fluorescence in the absence of POMs/POMds (■) or the presence of POM-Dawson (▲), POMds-Dawson-Co (●) or POMds-Dawson-Ni (▼). The data represented the means of three independent experiments. In contrast, we also tested the inhibition effect when POM-Dawson and Ni²⁺ were just mixed together (□). Error bars indicate \pm s.d. (b) Determination of the POMds on the formation of A β fibrils by native PAGE. Lane 1: control 1 (A β monomer only), lane 2: control 2 (A β 1–40 after incubation for 7 days), lane 3: A β 1–40/ POM-Dawson, lane 4: A β 1–40/POMds-Dawson-Co, lane 5: A β 1–40/POMds-Dawson-Ni.

Table 1 | Analysis of fluorescence titration, ITC and IC₅₀ data.

| Sample | Fluorescence titration* | | ITC | | IC ₅₀ [†] (μM) |
|-----------------|-----------------------------------|---|-----------------------------------|---|------------------------------------|
| | K _a (M ⁻¹) | ΔG _b (kJ mol ⁻¹) | K _a (M ⁻¹) | ΔG _b (kJ mol ⁻¹) | |
| POM-Dawson | (2.76 ± 0.11) × 10 ⁵ | – 31.05 ± 0.10 | 2.01 × 10 ⁵ | – 30.25 | 26.30 ± 4.32 |
| POMds-Dawson-Co | (9.70 ± 0.66) × 10 ⁵ | – 34.17 ± 0.41 | 9.07 × 10 ⁵ | – 33.99 | 14.73 ± 2.37 |
| POMds-Dawson-Ni | (1.77 ± 0.29) × 10 ⁶ | – 35.65 ± 0.17 | 1.68 × 10 ⁶ | – 35.51 | 5.67 ± 1.53 |

*Tyrosine-fluorescence titration data were used to estimate the binding constant by nonlinear least-squares fitting²⁰. ΔG_b = – RT ln K_a. The mean of three independent experiments with comparable results are shown. Error bars indicate \pm s.d.

[†]A ThT assay was used to estimate the average IC₅₀ value from three measurements. The mean values of three independent experiments with comparable results are shown. Error bars indicate \pm s.d.

The order of the inhibitory effects followed POMds-Dawson-Ni > POMds-Dawson-Co > POM-Dawson. This order was consistent with our quantitative thermodynamics results.

Recent evidence suggests that amyloid oligomers, which represent intermediates in the fibril formation process, are the main source of cytotoxicity by causing the death of neurons for amyloid pathogenesis, rather than the mature fibrils that accumulate as large aggregates^{41,42}. To verify the feasibility of the POMds for AD therapeutic applications, we studied their inhibitory effects on A β oligomers. The metal-induced oligomer of A β was prepared by treatment with Cu²⁺ at 37 °C for 24 h and determined by a native polyacrylamide gel electrophoresis (PAGE) assay (Supplementary Fig. 10)⁴². Lane 2 in Supplementary Fig. 10 shows that A β treated with Cu²⁺ alone had almost no monomer band. In contrast, A β oligomer formation was markedly inhibited by coincubating with POMds-Dawson-Co or POMds-Dawson-Ni, as shown by a stronger monomer band and a weaker aggregate band in the native gel (Supplementary Fig. 10, lanes 3–5). These findings indicated that A β oligomer aggregation was clearly inhibited and POMds-Dawson-Ni showed better effects.

To confirm the above electrophoresis results, metal-induced A β oligomers were studied by AFM (Supplementary Fig. 11). In the A β sample with Cu²⁺, a considerable amount of amorphous aggregates approximately 7 nm in size was detected after 24 h of incubation. While in the presence of POMds-Dawson-Co or POMds-Dawson-Ni, the A β oligomer was strongly inhibited, which could be observed as approximately 1.5 nm globules. A β monomers were determined as approximately 1.3 nm globules⁴³, whereas POMs could hardly be detected by AFM.

The binding site and stoichiometry between POMds and A β . As previously indicated, the binding site on which the initial

POM-Dawson located was the cationic cluster HHQK on A β ²³. For POMds-Dawson-Co or POMds-Dawson-Ni, the histidine-chelating effect would enhance the POMd binding to HHQK. In order to confirm the existence of the His-chelating effect between the POMds and A β monomer, we developed an amino acid-coated Fe₃O₄ binding assay (Supplementary Fig. 12A). For these experiments, a series of Fe₃O₄ coated with either glycine (Fe₃O₄@Gly), valine (Fe₃O₄@Val) or histidine (Fe₃O₄@His) was synthesized because the content of Gly and Val in A β are maximum compared with other amino acids. Each Fe₃O₄@amino acid was characterized as previously described (Supplementary Fig. 13)⁴⁴. Then, each amino acid-modified Fe₃O₄ was adequately incubated with different POM derivatives at several different concentrations for 1 h. The intermixtures were then treated with a magnet to separate the Fe₃O₄, and the supernatant was measured at 210 nm, which is the optimal absorption wavelength of POMs²³. According to the concentration curves of POM and POM derivatives in the supernatant (Supplementary Fig. 12B), Fe₃O₄@Gly and Fe₃O₄@Val hardly bound to the POM derivatives, indicating that the POM derivatives could not be located on these amino acid sites in A β . Due to electrostatic attraction effect, Fe₃O₄@His could bind to the POM derivatives. However, the affinities of the POMds were obviously stronger than that of POM-Dawson, especially for POMds-Dawson-Ni. Therefore, besides the electrostatic attraction, His-chelating effect also made favourable contribution. The above results suggested that the His-chelating effect did exist between the POMds and A β . When the POMds interacted with A β , they were prone to being located on the His sites in A β , especially on the HHQK cationic cluster because this site contained two adjacent histidines.

The stoichiometry for the complexation of POM/POMds with A β was first investigated by using Job's continuous variation method (Supplementary Fig. 14)⁴⁵. The intersection point

appeared at 0.5 in the plot, indicating that the binding stoichiometry of the POM/POMDs bound to A β was 1:1. MALDI-TOF MS was also used to study the POMDs binding to A β . After incubation of the POMDs and A β together at 4 °C for 60 min, the unique peak of the POMDs–A β complex could be easily detected, and the molecular weight was just equal to one POMDs plus one A β peptide (Supplementary Fig. 6A). Under the same conditions, the peak of the POM–A β complex was lower than that of the POMDs–A β compound (Supplementary Fig. 6B,C). The results indicated that the POM/POMDs bound to A β at a 1:1 ratio, and that the POMd binding to A β was stronger, which was verified by our next quantitative fluorescence titration experiments.

Next, we carried out an enzymatic digestion experiment with trypsin to investigate whether POM derivatives were located at the HHQK cluster on A β . Trypsin exclusively cleaves the C-terminal to arginine (R) and lysine (K) residues. We used the shorter fragment A β 12–28 with the sequence VHHQKL VFFAEDVGSNK, in which the enzyme digestion site and the POM derivatives binding site were at the same sequence. SDS–PAGE electrophoresis was used to determine whether A β was digested. The results showed that single A β was almost completely degraded after 10 min, whereas in the presence of POM–Dawson, POMDs–Dawson–Co or POMDs–Dawson–Ni at a 1:2 molar ratio with A β , proteolysis was weakened (Supplementary Fig. 15). Specifically, in the presence of POMDs–Dawson–Ni, the trypsin-induced degradation of lysozymes was barely affected. These results indicated that POM–Dawson, POMDs–Dawson–Co and POMDs–Dawson–Ni could interact with the A β monomer and protect it from trypsin-induced degradation, and that POMDs–Dawson–Ni provided the best protection. Furthermore, the POM derivatives were bound on the cationic cluster HHQK, which might play an important role in the specific binding of POM derivatives with A β . The above two results indicated that when interacted with A β , POMDs would bind to the HHQK cluster because this site was both positively charged and possessed His residues. These results were consistent with previous studies²³.

Molecular dynamic simulations provided further support for their binding. The geometry optimization algorithm was applied for each starting condition; molecular dynamic simulations were

then conducted using Autodock Vina until a stable complex was obtained⁴⁶. The best-fit obtained with this method is shown in Fig. 5. The POM-binding site of A β was identified as a cavity-like domain mainly encompassing the amino acids His13, Gln15 and Lys16 of A β 1–40. This domain of A β formed a relatively positively charged surface (Fig. 5b), which allowed the interactions with the negatively charged POM. The complex was further stabilized by two hydrogen bonds that involved His13–POM and Arg16–POM (Fig. 5c). This result also explained why POM did not bind at His6. There was no existing suitable cavity for recognizing POM around His6, and the amino acids around His6 were all negatively charged (such as Glu3, Asp7 and Ser8), which interfered with the interaction between His6 and POM (Fig. 5a).

Fluorescence titrations^{23,39,40} were used to estimate the binding constants of POM–Dawson, POMDs–Dawson–Co and POMDs–Dawson–Ni, which reflected the specificity between inhibitors and A β . With increasing POMDs–Dawson–Ni or POMDs–Dawson–Co, the fluorescence intensity of A β was quenched much stronger than that of POM–Dawson (Supplementary Fig. 16). The apparent binding constants, K_a , yielded by nonlinear least-squares fit^{39,40} showed that the K_a values of POMDs–Dawson–Ni and POMDs–Dawson–Co were approximately 6.44 and 3.52 times higher than that of POM–Dawson, respectively (Table 1). Furthermore, the binding free energy change was also estimated (Table 1). The binding free energy difference was approximately 4.6 kJ mol^{–1} between POMDs–Dawson–Ni and POM–Dawson. Together, these results indicated that Ni or Co in POMDs could enhance their binding affinity and recognition to A β with a defined binding site and improve the inhibition efficiency.

The stoichiometry and binding constant between POMDs and A β were confirmed by isothermal titration calorimetry (ITC; Fig. 6)^{47,48}. The binding was exothermic and best fit to a 1:1 binding model. Furthermore, the ITC data demonstrated that the binding constants of the POM–Dawson–A β , POMDs–Dawson–Co–A β and POMDs–Dawson–Ni–A β complexes were 2.01×10^5 , 9.07×10^5 and 1.68×10^6 , respectively. The binding free energy difference was approximately 5.26 kJ mol^{–1} between POMDs–Dawson–Ni and POM–Dawson, which indicated a higher affinity between POMDs and A β . These results were consistent with the fluorescence titration data (Table 1).

The binding site between A β and POMDs has been demonstrated to be the cationic cluster HHQK, not His or other single amino acids. The enhanced specific recognition between POMDs and A β could be attributed to two aspects. First, it was certainly attributed to the increased electrostatic attraction⁴⁹. Because POM–Dawson had six negative charges and the POMDs had eight, the additional negative charges could increase the electrostatic attraction towards the cationic cluster HHQK. Second, it could be the histidine-chelating effect, which improved the ability of the POMDs to recognize the HHQK cluster. It was clearly observed that, although POMDs–Dawson–Co and POMDs–Dawson–Ni had the same charges, the electrophoretic mobility of A β incubated with POMDs–Dawson–Ni was slower. Also, the value of the apparent binding constant K_a of POMDs–Dawson–Ni was larger than that of POMDs–Dawson–Co. These results demonstrated that the His-chelating effect between POMDs and HHQK existed and that POMDs–Dawson–Ni had the strongest interaction. According to all of the effects mentioned above, POMDs–Dawson–Ni showed the best specificity towards A β .

There are two possible mechanisms by which POMDs could inhibit A β aggregation more efficiently. The intense binding caused by electrostatic and histidine-chelating effects between POMDs and the A β monomer would substantially lower the concentration of the free monomer and shift the equilibrium

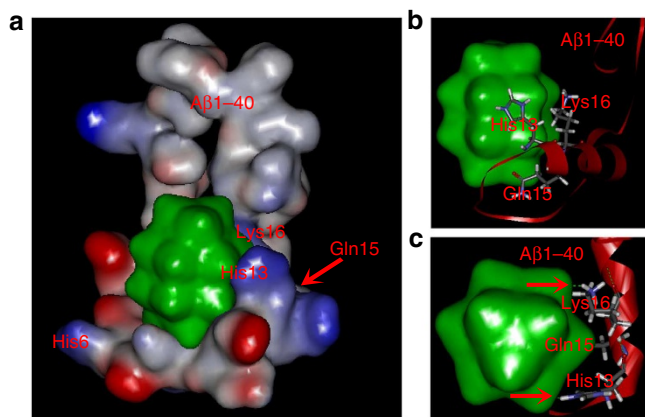


Figure 5 | Energy-minimized average model of POM–A β interactions.

This complex is shown in molecular surface models (a) and a tube representation (b,c) with POM in green. A remarkable feature of the model is that the POM-binding site of A β is identified as a positive electricity cavity-like domain mainly encompassed by His13, Gln15, Lys16 of A β 1–40. This is particularly visible in panel B. The complex is further stabilized by two hydrogen bonds, involving His13–POM and Arg16–POM. This is illustrated in c by arrows.

away from aggregation. In addition, it is possible that strong interactions between the POMds and A β oligomers could result in unfavourable conditions for nucleation and fibril growth through blocking direct contact between A β monomers. This situation would lead to the depletion of sub- and near-critical oligomers and to the partial blockage of the kinetic pathway until the surface is saturated and new nuclei can be grown^{39,40,50}.

Inhibition of A β -mediated peroxidase-like activity and cytotoxicity. Furthermore, it has been recently reported that haem binds to A β monomers, which may play another major role in AD (Fig. 7a)^{28–30}. In native human A β peptides, simultaneously mutating the His13 and His14 residues can prohibit haem binding and result in the loss of peroxidase-like activity. According to the above results, we took advantage of the electronegative and His-chelated POMds to show that the POMds-Dawson-Ni and POMds-Dawson-Co strongly targeted the HHQK cluster on A β , which blocked His13 and His14 simultaneously. Therefore, POMds could be outstanding inhibitors of the above peroxidase-like activity, and this hypothesis was confirmed. As described previously, haem-A β complexes showed remarkably enhanced peroxidase-like activity relative to free haem^{28–30}. When POM-Dawson was added to the system, the enhanced peroxidase-like activity still existed. However, when POMds-Dawson-Ni or POMds-Dawson-Co was added instead of POMds-Dawson at the same concentration, the enhanced peroxidase-like activity nearly disappeared (Fig. 7b, Supplementary Fig. 17). The results suggested that

POMds-Dawson-Ni and POMds-Dawson-Co acted as more effective inhibitors in depressing the A β -mediated peroxidase-like activity and they could be dual-functional agents for the treatment of AD.

Next, we further studied whether POMds-Dawson-Ni and POMds-Dawson-Co could inhibit A β -mediated cellular toxicity. To address this question, we used PC12 cells to probe cellular metabolism by using a 3-(4,5-dimethylthiazol-2-yl)-2,5-diphenyltetrazolium bromide (MTT) assay^{39,40}. A β was incubated in the presence or absence of POM-Dawson, POMds-Dawson-Ni or POMds-Dawson-Co for 7 days, and then the cells were exposed to the A β /POM mixtures. The data were normalized by using the results for cells not treated with A β fibrils as a positive control^{39,40}. In the presence of POM-Dawson or POMds, the survival of the cells significantly increased (Fig. 8a), indicating that POM-Dawson or POMds inhibited A β aggregation and decreased A β -induced cytotoxicity. POMds had a stronger effect than that of POM-Dawson. POMds-Dawson-Ni showed even better efficiency than POMds-Dawson-Co. At the same time, POM/POMds themselves were nontoxic at the same concentrations (Fig. 8b). Thus, POMds-Dawson-Ni and POMds-Dawson-Co could not only inhibit A β aggregation during *in vitro* studies, as evidenced by ThT fluorescence assay, but also decreased A β -induced cytotoxicity, which was consistent with our fluorescent live cell screening results.

Blood-brain barrier penetration. Due to the excellent profiles against A β fibril formation and A β -mediated peroxidase-like

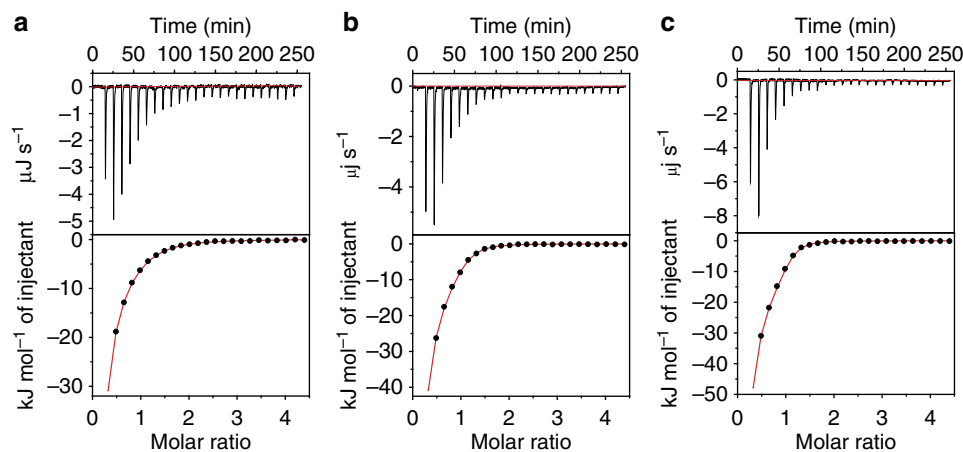


Figure 6 | Representative ITC data for the interactions between POM/POMds and A β . ITC titration curves of POM-Dawson (0.448 mM, **a**), POM-Dawson-Co (0.448 mM, **b**) and POM-Dawson-Ni (0.448 mM, **c**) with A β (0.02 mM) at 25 °C. Best-fit ITC values are listed in Table 1.

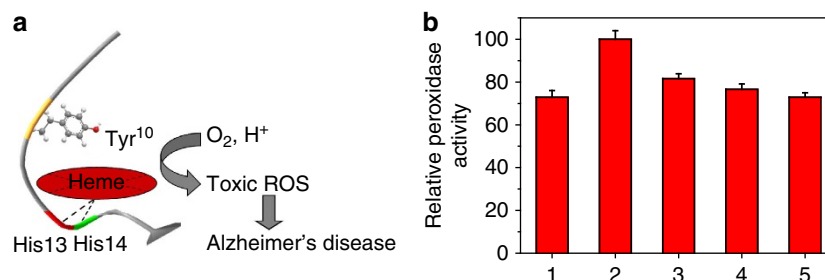


Figure 7 | Inhibition of A β -mediated peroxidase-like activity by POMds. (a) Schematic representation of A β -induced peroxidase-like activity generation. The haem-A β complexes, in which the haem is coordinated by His13 and His14, have been demonstrated to function as peroxidases. (b) Effect of POMds on the inhibition of A β -induced peroxidase-like activity, monitoring the increase of the 420 nm absorbance intensity after 200 s, for different haem-A β -POMds complexes: free haem (1); haem + A β (2); haem + A β + POM-Dawson (3); haem + A β + POMds-Dawson-Co (4); haem + A β + POMds-Dawson-Ni (5). The experiment was repeated three times. Error bars indicate \pm s.d.

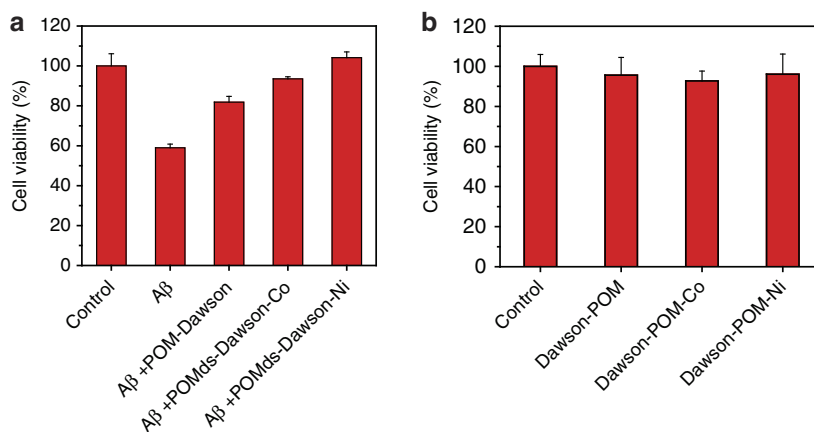


Figure 8 | Effect of POMds on cell toxicity of A β . Samples were prepared in the presence (a) or absence (b) of POM/POMds. The cytotoxic effect on PC12 cells was determined by using MTT assay from three separate measurements. Each experiment had been repeated three times. Error bars indicate \pm s.d.

activity *in vitro*, POMds may be suitable for generating a bio-available drug in the treatment of AD. A major impediment to the development of effective anti-A β compounds for AD therapy is that essentially 100% of large-molecule drugs and >98% of small-molecule drugs fail to cross the blood-brain barrier (BBB)⁵¹. To ensure that the POMds could cross the BBB, we treated wild-type mice with POMds-Dawson-Ni, which had the best effect. Each mouse was intravenously administered 25 mg of POMds-Dawson-Ni per kilogram of body weight. Blood and brain tissue were collected at 5, 10, 30 and 60 min post dosing; plasma was then separated from the blood and the brain tissue was homogenized. As a surrogate measure of drug levels, plasma and brain homogenates were analysed for levels of tungsten by inductively coupled plasma mass spectrometry (ICP-MS). As predicted, the levels of W in the plasma rapidly increased to the peak level in the animals treated with POMds-Dawson-Ni after 5 min (approximately 8.91 mg kg⁻¹). Notably, the highest level of W in the brain did not appear at the same time as in the plasma, but rather, at 10 min after dosing (approximately 0.0231 mg kg⁻¹) (Supplementary Fig. 18). Thereafter, the concentrations of W markedly decreased in both the plasma and brain. After 60 min, only 1.0 and 9.6% of W remained in the plasma and brain, respectively, compared with each peak value. After 48 h, the concentrations of W in both the plasma and brain returned to the initial levels. We used mice treated with only physiological saline as controls; the concentrations of W and Ni in the brains were too low to measure.

The *in vivo* stability of POMds was also evaluated. We treated wild-type Wistar rats with POMds-Dawson-Ni. Each rat was intravenously administered 25 mg of POMds-Dawson-Ni per kilogram of body weight. Brain tissues were collected at 60 min post dosing and homogenized. The brain homogenates were analysed by high-performance liquid chromatography (HPLC). As shown in Supplementary Fig. 19A, the samples had POMds-Dawson-Ni peaks at the same retention time as POMds-Dawson-Ni alone. We also used ICP-MS to study the *in vivo* stability. The measured Ni/W weight ratio was 1:52.11, and the calculated value was 1:53.25. Both results indicated that POMds-Dawson-Ni was not only permeable but also stable *in vivo*.

Since AD is characterized by cerebral extracellular amyloid plaques, the distribution of POMds in brain tissues should be determined. We treated wild-type Wistar rats with POMds-Dawson-Ni, and each rat was intravenously administered 25 mg of POMds-Dawson-Ni per kilogram of body weight. The cerebrospinal fluids were collected at 60 min after dosing and

then centrifuged. The supernatants were also analysed by HPLC. As predicted, the samples had the POMds-Dawson-Ni peaks at the same retention times as those of POMds-Dawson-Ni alone (Supplementary Fig. 19B). These findings indicated that POMds-Dawson-Ni could distribute extracellularly in the brain, where A β aggregates predominately exist. The HPLC results further confirmed that POM-Dawson-Ni could cross the BBB and remain intact *in vivo*.

In summary, by using a high-throughput screening method based on the fluorescence of an A β -ECFP fusion expression system, a ThT fluorescence assay, PC12 cell toxicity and quantitative thermodynamics studies, our designed and synthesized transition metal-functionalized POMds show an improved A β inhibitory effect compared with the Wells-Dawson-type POM. A Ni-metallated POM derivative can achieve a sixfold improvement. Transition metal-functionalized POMds with defined histidine-chelated binding sites can not only specifically target the HHQK cluster of A β with improved cytotoxicity but also show stronger inhibitory effects through enhanced A β binding affinity, as evidenced by the quantitative thermodynamic studies. Moreover, the POMds-Dawson-Ni and POMds-Dawson-Co exhibit better effects for depressing the A β -mediated peroxidase-like activity, indicating that our designed and synthesized POMds can be dual-functional therapeutic agents against AD. Furthermore, the POMds can cross the BBB and be metabolized after 48 h. In this sense, our work advances our understanding of the design and synthesis of inorganic metal compounds as multifunctional therapeutic agents against AD.

Methods

Sample preparation. A β 1-40 was purchased from American Peptide (Sunnyvale, California, USA, lot no. U10012). Peptides were prepared as previously described²³. Briefly, the powdered A β peptide was first dissolved in 1,1,1,3,3,3-hexafluoro-2-propanol at a concentration of 1 mg ml⁻¹. The solution was shaken at 4 °C for 2 h in a sealed vial for further dissolution and then stored at -20 °C as a stock solution. Before use, the solvent 1,1,1,3,3,3-hexafluoro-2-propanol was removed by evaporation under a gentle stream of nitrogen, and the peptide was dissolved in 10 mM of HEPES buffer (pH 7.4, containing 150 mM of NaCl).

High-throughput screening of A β inhibitors. Briefly, the *Escherichia coli* strain BL21(DE3) was transformed by the vector ALC (A β -linker-ECFP) or the control vector CFP (linker-ECFP) and cultured at 37 °C in lysogeny broth (LB, pH 7.4) containing ampicillin (50 μ g ml⁻¹). Different POMs or POMds were added to the culture medium 30 min prior to protein expression induced by isopropyl- β -D-1-thiogalactopyranoside (1 mM). After expression of the recombinant proteins for 3 h, all samples were diluted to an optical density of 0.1 at 600 nm. The fluorescence of each sample was measured at 512 nm (excitation 433 nm) with a JASCO FP6500

spectrofluorometer. Compounds were tested in triplicate at a final concentration of 100 μM (ref. 52).

ThT fluorescence spectroscopy. The kinetics of A β aggregation was monitored using the dye ThT, the fluorescence of which is dependent on the formation of amyloid fibrils. Fluorescence measurements were carried out with a JASCO FP6500 spectrofluorometer. The fluorescence signal (excitation at 444 nm) was recorded between 460 and 650 nm; 10 nm slits were used for both emission and excitation measurements. The peptide concentration was 1 μM , and the ThT concentration was 10 μM . At different times, aliquots of the A β solution were taken for fluorescence measurements.

AFM study. For the AFM measurements, samples were diluted with deionized H₂O to yield a final concentration of 1 μM . Next, the sample (20 μl) was applied to freshly cleaved muscovite mica and allowed to dry. Data were acquired in the tapping mode on a Nanoscope V multimode atomic force microscope (Veeco Instruments, USA). The resonance frequency was 358.305 Hz, and the scanning frequency was 0.996 Hz. Homoeothermic equipment was used to maintain the temperature during the scan.

Native gel electrophoresis. Samples (10 μl) were analysed by 12% native PAGE. Gels were run in a Tris/glycine system and developed by the silver-stain method.

Fluorescence titration. The binding constants of POMds with A β were determined by fluorescence titration at 25 °C. The excitation wavelength was 278 nm, and the emission intensity at 306 nm was monitored as a function of continuous increasing concentrations of POMds. The A β 40 peptide concentration was fixed at 3 μM , whereas the POMds concentration was varied between 0–5.5 μM . The 1:1 binding stoichiometric equation was used to calculate the binding constants^{39,40}.

Amino acid-coated Fe₃O₄ binding assay. To an aqueous solution of a mixture of Fe(III) and Fe(II) salts, an amino acid solution in the molar ratio 2Fe(III):1Fe(II):4 amino acids was added and maintained at a constant temperature of 40 °C for 15 min under vigorous stirring. Next, a solution of ammonium hydroxide was added until the pH was increased to approximately 11, at which point a black suspension formed. This suspension was then refluxed at 80 °C for 6 h under vigorous stirring. The amino acid-coated Fe₃O₄ were separated from the aqueous solution by magnetic decantation, washed with distilled water several times and then dried in an oven overnight. Each amino acid-modified Fe₃O₄ was adequately incubated with different POM derivatives at several different concentrations for one hour. The intermixtures were then treated with a magnet to separate Fe₃O₄, and the supernatant was measured at 210 nm (ref. 44).

Trypsin digestion. A β (20 μM) was preincubated in 10 mM Tris buffer (pH 7.4) in the absence or presence of POM (in 2:1 A β /POM ratios) for 30 min at 37 °C; it was then subjected to proteolysis by trypsin (0.1 mg ml⁻¹) under the same conditions for 10 min. At the end of the reaction, all samples were supplemented with native PAGE reducing sample buffer, carefully heated at 100 °C for 5 min and subjected to native PAGE (20%). The gels were then silver-stained.

Isothermal Titration Calorimetry. ITC assays were performed on a NANO ITC System (TA Instruments Inc., New Castle, Delaware, USA). Titrations were performed in buffer (10 mM HEPES buffer, 150 mM NaCl, pH = 7.4). Injections of 10 μl of 0.45 mM POM or POMds were added from a computer-controlled microsyringe at an interval of 600 s into an A β (20 μM) solution, with stirring at 400 r.p.m. at 25 °C. The experimental data were analysed with NanoAnalyze software (TA Instruments Inc.) and were fitted to an independent model concurrently with a blank constant model to adjust for the heat of dilution. All measurements were obtained from 25 injections of 0.45 mM POM or POMds into 1400 μl of A β in 10 mM HEPES, 150 mM NaCl, pH = 7.4 buffer at 25 °C. Each heat-burst curve was the result of a 10 μl injection of POM or POMds into the A β solution.

³¹P NMR and MALDI-TOF MS. ³¹P NMR spectroscopy measurements were carried out on a Bruker Avance 600 MHz NMR spectrometer at 10 °C. POM samples were dissolved in D₂O. Experimental conditions were according to Lyou *et al.*³² Samples were deposited on the MALDI target using a dried droplet method²⁴. MALDI-TOF MS experiments were performed in positive ion mode on an Autoflex III TOF/TOF analyser (Bruker Daltonics Inc., Germany) with the Nd-YAG laser operated at 355 nm with 0 ns duration pulses, a repetition rate of 200 Hz and an acceleration voltage of 19 kV. MS spectra were acquired as an average of 100 laser shots for two times. The laser intensity presented here was defined as 45% of the total laser intensity according to the practical instrument condition.

Inhibition of A β -mediated peroxidase-like activity and cytotoxicity assays.

The inhibition assay was performed as previously described^{28–30}. Cytotoxicity was measured as follows. PC12 cells (rat pheochromocytoma, American Type Culture Collection) were cultured in Iscove-modified Dulbecco's medium (Gibco BRL) supplemented with 5% foetal bovine serum and 10% horse serum in a humidified 5% CO₂ environment at 37 °C. Cells were plated at a density of 10,000 cells per well on 96-well plates in fresh medium (90 ml). After 24 h, A β 1–40 peptides (5 μM) that had been aged with or without POMs were added, and the cells were further incubated for 48 h at 37 °C. Cytotoxicity was measured using a modified MTT assay kit (Promega). The absorbance values of formazan were determined at 490 nm with an automatic plate reader.

Blood – brain barrier penetration assay. POMds-Dawson-Ni in saline was intravenously administered to wild-type mice through a tail vein injection at 25 mg · kg⁻¹ body weight. Brain tissues were collected at 5, 10, 30 and 60 min after dosing; the plasma was then separated from the blood, and the brain tissue was homogenized. As a surrogate measure of drug levels, the plasma and brain homogenates were analysed for levels of tungsten by ICP-MS⁵².

References

- Haass, C. & Selkoe, D. J. Soluble protein oligomers in neurodegeneration: lessons from the Alzheimer's amyloid β -peptide. *Nat. Rev. Mol. Cell Biol.* **8**, 101–112 (2007).
- Gotz, J. & Ittner, L. M. Animal models of Alzheimer's disease and frontotemporal dementia. *Nat. Rev. Neurosci.* **9**, 532–544 (2008).
- Geng, J., Li, M., Wu, L., Ren, J. & Qu, X. Liberation of copper from amyloid plaques: making a risk factor useful for Alzheimer's disease treatment. *J. Med. Chem.* **55**, 9146–9155 (2012).
- Wang, D. & Lippard, S. J. Cellular processing of platinum anticancer drugs. *Nat. Rev. Drug. Discov.* **4**, 307–320 (2005).
- Orvig, C. & Abrams, M. J. Medicinal inorganic chemistry: introduction. *Chem. Rev.* **99**, 2201–2214 (1999).
- Barnham, K. J. *et al.* Platinum-based inhibitors of amyloid- β as therapeutic agents for Alzheimer's disease. *Proc. Natl Acad. Sci. USA* **105**, 6813–6818 (2008).
- Kim, J. E. & Lee, M. Fullerene inhibits β -amyloid peptide aggregation. *Biochem. Biophys. Res. Commun.* **303**, 576–579 (2003).
- Prudent, R., Sautel, C. F. & Cochet, C. Structure-based discovery of small molecules targeting different surfaces of protein-kinase CK2. *Biochim. Biophys. Acta* **1804**, 493–498 (2010).
- Yanagie, H. *et al.* Anticancer activity of polyoxomolybdate. *Biomed. Pharmacother.* **60**, 349–352 (2006).
- Hasenknopf, B. Polyoxometalates: introduction to a class of inorganic compounds and their biomedical applications. *Front. Biosci.* **10**, 275–287 (2005).
- Rhule, J. T., Hill, C. L., Judd, D. A. & Schinazi, R. F. Polyoxometalates in medicine. *Chem. Rev.* **98**, 327–357 (1998).
- Judd, D. A. *et al.* Polyoxometalate HIV-1 protease inhibitors. A new mode of protease inhibition. *J. Am. Chem. Soc.* **123**, 886–897 (2001).
- Sarafianos, S. G., Kortz, U., Pope, M. T. & Modak, M. J. Mechanism of polyoxometalate-mediated inactivation of DNA polymerases: an analysis with HIV-1 reverse transcriptase indicates specificity for the DNA-binding cleft. *Biochem. J.* **319**, 619–626 (1996).
- Seko, A., Yamase, T. & Yamashita, K. Polyoxometalates as effective inhibitors for sialyl- and sulfotransferases. *J. Inorg. Biochem.* **103**, 1061–1066 (2009).
- Wu, Q., Wang, J., Zhang, L., Hong, A. & Ren, J. Molecular recognition of basic fibroblast growth factor by polyoxometalates. *Angew. Chem. Int. Ed.* **44**, 4048–4052 (2005).
- Pope, M. T. & Kortz, U. Polyoxometalates. *Encyclopedia Inorg. Bioinorg. Chem.* 1–14 (2012).
- Nohra, B. *et al.* Polyoxometalate-based metal organic frameworks (POMOFs): structural trends, energetics, and high electrocatalytic efficiency for hydrogen evolution reaction. *J. Am. Chem. Soc.* **133**, 13363–13374 (2011).
- Allain, C. *et al.* Synthesis, electrochemical and photophysical properties of covalently linked porphyrin–polyoxometalates. *Dalton Trans.* **42**, 2745–2754 (2013).
- Micoine, K., Hasenknopf, B., Thorimbert, S., Lacote, E. & Malacria, M. Chiral recognition of hybrid metal oxide by peptides. *Angew. Chem. Int. Ed.* **121**, 3518–3520 (2009).
- Geisberger, G., Paulus, S., Gyenge, E. B., Maake, C. & Patzke, G. R. Targeted delivery of polyoxometalate nanocomposites. *Small* **7**, 2808–2814 (2011).
- Flutsch, A., Schroeder, T., Grutter, M. G. & Patzke, G. R. HIV-1 protease inhibition potential of functionalized polyoxometalates. *Bioorg. Med. Chem. Lett.* **21**, 1162–1166 (2011).
- Narasimhan, K. *et al.* Identification of a polyoxometalate inhibitor of the DNA binding activity of Sox2. *ACS Chem. Biol.* **6**, 573–581 (2011).

23. Geng, J., Li, M., Ren, J., Wang, E. & Qu, X. Polyoxometalates as inhibitors of the aggregation of amyloid β peptides associated with Alzheimer's disease. *Angew. Chem. Int. Ed.* **50**, 4184–4188 (2011).
24. Liu, Z. *et al.* The use of multifunctional magnetic mesoporous core/shell heteronanostructures in a biomolecule separation system. *Biomaterials* **32**, 4683–4690 (2011).
25. Harney, A. S. *et al.* Targeted inhibition of Snail family zinc finger transcription factors by oligonucleotide-Co(III) Schiff base conjugate. *Proc. Natl Acad. Sci. USA* **106**, 13667–13672 (2009).
26. Haas, K. L. & Franz, K. J. Application of metal coordination chemistry to explore and manipulate cell biology. *Chem. Rev.* **109**, 4921–4960 (2009).
27. Man, B. Y.-W. *et al.* Group 9 metal-based inhibitors of β -amyloid (1–40) fibrillation as potential therapeutic agents for Alzheimer's disease. *Chem. Sci.* **2**, 917–921 (2011).
28. Pramanik, D., Ghosh, C. & Dey, S. G. Haem-Cu bound A β peptides: spectroscopic characterization, reactivity, and relevance to Alzheimer's disease. *J. Am. Chem. Soc.* **133**, 15545–15552 (2011).
29. Cassagnes, L. E. *et al.* The catalytically active copper-amyloid-beta state: coordination site responsible for reactive oxygen species production. *Angew. Chem.* **125**, 11316–11319 (2013).
30. Pedersen, J. T. *et al.* Rapid exchange of metal between Zn7-metallothionein-3 and amyloid- β peptide promotes amyloid-related structural changes. *Biochemistry* **51**, 1697–1706 (2012).
31. Pirie, C. M., Mey, M. D., Prather, K. L. J. & Ajikumar, P. K. Integrating the protein and metabolic engineering toolkits for next-generation chemical biosynthesis. *ACS Chem. Biol.* **8**, 662–672 (2013).
32. Lyon, D. K. *et al.* Highly oxidation resistant inorganic-porphyrin analogue polyoxometalate oxidation catalysts. *J. Am. Chem. Soc.* **113**, 7209–7221 (1991).
33. Kim, W. *et al.* A high-throughput screen for compounds that inhibit aggregation of the Alzheimer's peptide. *ACS Chem. Biol.* **1**, 461–469 (2006).
34. LeVine, III H. T. Thioflavine. *Protein Sci.* **2**, 404–410 (1993).
35. Geng, J., Zhao, C., Ren, J. & Qu, X. Alzheimer's disease amyloid beta converting left-handed Z-DNA back to right-handed B-form. *Chem. Commun.* **46**, 7187–7189 (2010).
36. Yu, H., Ren, J. & Qu, X. Time-dependent DNA condensation induced by amyloid β -peptide. *Biophys. J.* **92**, 185–191 (2007).
37. Co, N. T., Hu, C. K. & Li, M. S. Dual effect of crowders on fibrillation kinetics of polypeptide chains revealed by lattice models. *J. Chem. Phys.* **138**, 185101–185105 (2013).
38. Soto, C. *et al.* β -sheet breaker peptides inhibit fibrillogenesis in a rat brain model of amyloidosis: implications for Alzheimer's therapy. *Nat. Med.* **4**, 822–826 (1998).
39. Yu, H. *et al.* Metallosupramolecular complex targeting an α/β discordant stretch of amyloid β peptide. *Chem. Sci.* **3**, 3145–3153 (2012).
40. Yu, H., Ren, J. & Qu, X. Different hydration changes accompanying copper and zinc binding to amyloid β -peptide: water contribution to metal binding. *Chem. Bio. Chem.* **9**, 879–882 (2008).
41. Walsh, D. M. & Teplow, D. B. Alzheimer's disease and the amyloid β -protein. *Prog. Mol. Biol. Transl. Sci.* **107**, 101–124 (2012).
42. Geng, J., Li, M., Wu, L., Chen, C. & Qu, X. Mesoporous silica nanoparticle-based H₂O₂ responsive controlled-release system used for Alzheimer's disease treatment. *Adv. Healthc. Mater.* **1**, 332–336 (2012).
43. Giuffrida, M. L. *et al.* β -amyloid monomers are neuroprotective. *J. Neurosci.* **29**, 10582–10587 (2009).
44. Unal, B. *et al.* L-histidine coated iron oxide nanoparticles: synthesis, structural and conductivity characterization. *J. Alloy. Compd* **505**, 172–178 (2010).
45. Ipe, B. I., Yoosaf, K. & Thomas, K. G. Functionalized gold nanoparticles as phosphorescent nanomaterials and sensors. *J. Am. Chem. Soc.* **128**, 1907–1913 (2006).
46. Trott, O. & Olson, A. J. AutoDock Vina: improving the speed and accuracy of docking with a new scoring function, efficient optimization, and multithreading. *J. Comput. Chem.* **31**, 455–461 (2010).
47. Zawisza, I., Rozga, M. & Bal, W. Affinity of copper and zinc ions to proteins and peptides related to neurodegenerative conditions (A β , APP, α -synuclein, PrP). *Coord. Chem. Rev.* **256**, 2297–2307 (2012).
48. Zhou, Y. *et al.* Inhibition of amyloid- β protein fibrillation upon interaction with polyoxometalates nanoclusters. *Colloids and Surfaces A: Physicochem. Eng. Aspects* **375**, 97–101 (2011).
49. Stroobants, K. *et al.* Polyoxometalates as a novel class of artificial proteases: selective hydrolysis of lysozyme under physiological pH and temperature promoted by a cerium(IV) Keggin-type polyoxometalate. *Chem. Eur. J.* **19**, 2848–2858 (2013).
50. Cabaleiro-Lago, C. *et al.* Inhibition of amyloid β protein fibrillation by polymeric nanoparticles. *J. Am. Chem. Soc.* **130**, 15437–15443 (2008).
51. Pardridge, W. M. Alzheimer's disease drug development and the problem of the blood-brain barrier. *Alzheimer's Dement* **5**, 427–432 (2009).
52. Lee, J. *et al.* On-demand drug release system for *in vivo* cancer treatment through self-assembled magnetic nanoparticles. *Angew. Chem. Int. Ed.* **125**, 4480–4484 (2013).

Acknowledgements

This work was supported by 973 Project (2011CB936004, 2012CB720602) and NSFC (21210002, 91213302).

Author contributions

J.R. and X.Q. designed the research; N.G., H.S., K.D., T.D. and C.X. performed the research; N.G., H.S., K.D. and C.X. analysed the data; J.R. and X.Q. wrote the paper.

Additional information

Supplementary Information accompanies this paper at <http://www.nature.com/naturecommunications>

Competing financial interests: The authors declare no competing financial interests.

Reprints and permission information is available online at <http://www.npg.nature.com/reprintsandpermissions/>

How to cite this article: Gao, N. *et al.* Transition-metal-substituted polyoxometalate derivatives as functional anti-amyloid agents for Alzheimer's disease. *Nat. Commun.* 5:3422 doi: 10.1038/ncomms4422 (2014).